量子色力学類似有効理論に於けるカラー超伝導体の熱力学

木内一佳志

了徳寺大学・健康科学部・医学教育センター

要旨

クォークとグルオンの物理系は、低温・低密度では、カイラル対称性の破れたハドロン相となっているが、高温、若しくは高密度では、カイラル対称性が回復し、クォーク・グルオン・プラズマ相（QGP）あるいは、カラー超伝導相などとなる。

今回われわれは、有限温度および密度に於いて、２フレーバーカラー超伝導体 (2SC) の熱力学を量子色力学類似有効理論を用いて調べた。中等度のクォーク密度領域に於いて $2\Delta^{T=0}_{p=p_F} = 3.43 k_B T_c$ という結果を得た (Δ:ギャップエネルギー, p_F:フェルミ運動量、k_B:ボルツマン定数, T_c:臨界温度)。この値は、通常の電子系の超伝導での結果 ($2\Delta = 3.52 k_B T_c$) と略同じである。クォーク・クーパー対の波動関数は規格化定数を別にすれば、温度に依存せず、対のコヒーレンス長は、臨界温度まで略一定であることが判明した。　一方、エネルギーギャップは、温度の上昇と共に減少し、臨界温度で零となる。従って、2SC から QGP への 2 次相転移は、クォーク・クーパー対の空間構造の不変性と対の減少によって特徴付けられることが判った。

キーワード: 有限温度、熱力学、カラー超伝導体、QCD 類似理論、クーパー対

Thermodynamics of Color Superconductor in a QCD-like Effective Theory

Hiyoshi KIUCHI
Faculty of Health Science, Ryotokuji University

abstract

We have investigated the thermodynamics of two-flavor color superconductor (2SC) at finite temperature (T) and quark chemical potential (μ) within the framework of a QCD-like effective theory, in which an asymptotically free momentum-dependent running coupling is used. Two kinds of systems have been investigated. One is with a tree-level gluon propagator (model A) and the other is with the lattice-QCD based (LQB) gluon propagator (model B). We have found that $2\Delta^{T=0}_{p=p_F} = 3.43 k_B T_c$ in model B (Δ:energy gap, k_B:Boltzmann constant, T_c:critical temperature). This value is very close to the famous BCS result, which is $2\Delta = 3.52 k_B T_c$. We have found that the coherence length (η) is not affected by T in 2SC, while Δ decreases as T increases and vanishes at T_c. In addition, we have found that the Cooper pair wave function $\Phi(p)$ is not affected by T, apart from normalization constant. With these results, the second-order phase transition between 2SC and a normal quark matter, which is considered to be quark-gluon plasma, can be characterized by the constant spatial structure and decrease in the coherent Cooper pair number with increased T. The quark density of the 2SC has been found to be in a realistic region for compact star core. The value of η in 2SC is shorter than the averaged interquark density (d). The small size of the Cooper pair suggests that they are tightly bound and rather bosonic. Therefore, it is natural that we expect the realizability of quark Bose-Einstein condensation phase. Some of our results, those are the larger Δ, higher T_c, wider μ region and shorter η in model B, suggest that the LQB gluon propagator induces stronger quark-quark interaction than the tree-level one.

Key words: thermodynamics, color superconductor, QCD-like theory, Cooper pair

I . Introduction

In our current understanding of nuclear physics, strong interactions are ruled by quantum chromodynamics (QCD), which is one of non-Abelian gauge field theories. According to QCD, quark-(anti-)quark interaction is induced by gluon (the gauge boson in QCD) exchange.

The QCD Lagrangian is invariant under $SU(3)$ gauge transformation in color space. We find that the QCD Lagrangian is difficult to handle without approximation, apart from its appearance. Under the circumstance, some simpler theories or models have been used for exploring QCD, such as the Nambu-Jona-Lasinio model[1)–3)], the instanton vacuum model[4)–6)], the quark-meson model[7)] and the QCD-like theory[8)–11)].

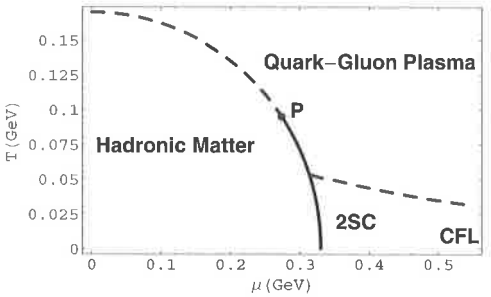

Figure 1: A schematic representation of the expected phase diagram of QCD matter on the T-μ plane. 2SC and CFL denote two-flavour colour superconducting and colour-flavour locking phases, respectively.

Mapping the phase diagram of QCD is one of the most fundamentally interesting subject in the field of strong interaction physics. At low temperature (T) and quark chemical potential (μ), a system of quarks and gluons lies in hadronic phase in which chiral symmetry is spontaneously broken. Recent progress has revealed that the chiral symmetry can be restored, and quarks and gluons will become deconfined at high T and/or μ. In addition, it is expected that quark matter at low T has a rich phase structure including color superconducting phase, where the quarks form Cooper pairs, such as two-flavor color superconducting phase (2SC) and color-flavor locking phase (CFL)[12)–14)]. In the color superconducting phases, color symmetry is spontaneously broken.

A typical schematic picture of the QCD phase diagram is presented in Fig. 1. The dashed and solid lines are phase transition lines. Due to the generalized Clapeyron-Clausius relation, the dashed line is perpendicular to the longitudinal axis at $\mu = 0$ and the solid line is perpendicular to the transverse axis at $T = 0$[15)]. Reliable informations along the $\mu = 0$ line are available from lattice gauge calculations[16)]. While, informations of finite μ region are available from the above mentioned theoretical studies. For instance, for $N_f = 2$ in the chiral limit, the dashed lines mean second-order phase transition lines and the solid line means a first-order phase transition line. We have a second-order phase transition between hadronic matter (HM) and quark-gluon plasma (QGP) at about $T = 0.17$ GeV along the $\mu = 0$ line, and a first-order phase transition between HM and 2SC at about $\mu = 0.3$ GeV (moderate quark density) along the $T = 0$ line. The tricritical point 'P' links up the second-order phase transition line to the first-order phase transition line.

The main subject of the present study is to investigate thermodynamics of 2SC in moderate μ region at finite T within the framework of a QCD-like gauge field theory, in which an asymptotically free momentum-dependent running coupling is used. In addition, we investigate effect of lattice-QCD based (LQB) gluon propagator on the thermodynamics. The propagator is considered to include all the nonperturbative effects in the quenched QCD. To the purpose, we combine the QCD-like theory and the LQB gluon propagator in three-momentum space[17)].

In the present study, we ignore the chiral symmetry broken phase and consider the matter as the chirally symmetric system.

There have been a few reports using the QCD-like theory with a similar one-loop running

coupling. However, all of them was performed in four dimensional space and limited to the case at $T = 0$.

In the universe, we may expect that such quark matters as 2SC and CFL exist inside compact stars[18),19)]. In addition, based upon compact star phenomenology, 2SC can be more important than CFL. Since the latter requires approximate flavor $SU(3)$ symmetry, the relevant region is at $\mu > 0.45$ GeV, of the order of strange quark mass, whereas at the center of typical compact star, μ is expected not to exceed 0.5 GeV (quark density might be as large as $10\rho_0$, where the nuclear matter density $\rho_0 \sim 0.46$ fm^{-3})[19)]. In addition, it has shown that, if compact star core is CFL, it is difficult to explain the majority of the X-ray data about existing compact stars. While, 2SC is allowed to exist in the core. Because in the CFL cases, the cooling of the compact star temperature is too fast in comparison with the observation data.[20)]

Throughout the paper, because strange quark is not important at low to moderate μ, we restrict ourselves to $N_f = 2$, corresponding to a system of only up and down quarks. The two-flavor quark matter is unstable with respect to the formation of quark-quark (q-q) Cooper pair condensate. The q-q interaction is most attractive in the Lorentz scalar, total spin singlet ($J = 0$), color anti-triplet ($\bar{3}$) and flavor anti-symmetric channel(see Appendix 8.1.3). Consequently, nonzero diquark condensate $\langle qC\gamma_5 q\rangle$ breaks color $SU(3)$ symmetry down to $SU(2)$ symmetry[21)].

The outline of the paper is as follows. In the next section, we derive the gap equation for momentum-dependent diquark energy gap $\Delta_{\mathbf{p}}$ at finite T in the mean-field approximation. In section 3, we give the equation for coherence length. In section 4, we derive the thermodynamic potential at finite T. In section 5, we give the equation for quark density and occupation number. In section 6, we solve the gap equation and compute Cooper pair wave function, the coherence length and some thermodynamic quantities in two kinds of system, and present the numerical results. Section 7 is devoted to conclusion.

II. Gap equation

In this section, we derive a gap equation of a quark superconducting state, which is called color superconductor, for two flavors at finite temperature in mean-field approximation. In the ordinary superconductor, electron Cooper pair is induced by phonon. While in color superconductor, quark Cooper pair is induced by gluon.

Let us start with an effective Hamiltonian with gluon exchange interaction.

$$H = H_0 + H_I, \tag{1}$$

where

$$H_0 = \int d^3x \overline{\Psi}(x)(i\nabla\!\!\!/ - \mu\gamma_0 - m)\Psi(x), \tag{2}$$

$$H_I = K\int d^3x d^3y \frac{g^2}{2}\overline{\Psi}(x)\gamma_\mu\frac{\lambda^A}{2}\Psi(x)D(x-y)\overline{\Psi}(y)\gamma^\mu\frac{\lambda^A}{2}\Psi(y), \tag{3}$$

with current quark mass m, quark chemical potential μ, the coupling constant g^2, a coefficient K and the color $SU(3)$ matrices λ^A. Here, the function $D(x-y)$ is a gluon propagator, which is given by

$$D(x-y) = \int \frac{d^3p}{(2\pi)^3}\frac{d(p^2)}{p^2}\mathrm{e}^{-ip(x-y)}, \tag{4}$$

where $d(p^2)$ is the polarization factor.

In this study, for the polarization factor, we adopt that of the LQB gluon propagator which is derived using the quenched lattice QCD data. Usual choice of the polarization factor in the QCD-like theory is that of the tree-level gluon propagator, i.e., $[d(p^2) = 1]$.

The polarization factor $d(p^2)$ of the lattice-QCD-based gluon propagator is well described by the following analytic function[17),22)] :

$$d(p^2) = Z_g \frac{p^4 + ap^2}{p^4 + \alpha p^2 + \beta}, \tag{5}$$

where $p \equiv |\mathbf{p}|$, $a = 7.887$ GeV^2, $\alpha = 1.254$ GeV^2, $\beta = 0.7175$ GeV^4 and $Z_g = 0.7172$ (Fig. 1).

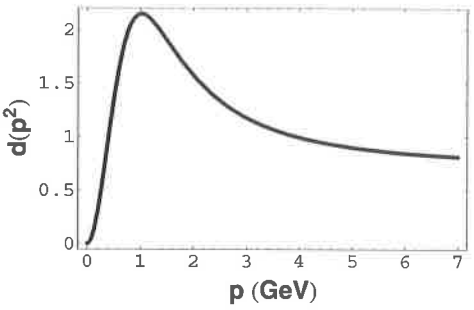

Figure 2: The polarization factor $d(p^2)$ of the lattice-QCD-based gluon propagator as a function of transfer momentum p exhibits the infrared vanishing and strong enhancement at the intermediate-energy region $p \sim 1$ GeV.

In this study, we concentrate on the Lorentz scalar $qC\gamma_5 q(\bar{q}C^\dagger\gamma_5\bar{q})$ bilinears in two-flavour quark matter.

In $2SC$ phase, diquark condensate consists of only two of the three colors[21)]. Then, the Fierz-rearranged Hamiltonian in 3-momentum space for two flavors is given by

$$\hat{H} = \hat{H}_0 + \hat{H}_I, \tag{6}$$

where

$$\hat{H}_0 \equiv \sum_{\mathbf{p}} (e_{\mathbf{p}} - \mu) C_R^{\dagger\alpha,s}(\mathbf{p}) C_R^{\alpha,s}(\mathbf{p}) + R \to L, \tag{7}$$

$$\begin{aligned} \hat{H}_I \equiv & -\frac{K}{3} g^2 \sum_{\mathbf{p},\mathbf{p}'} D(\mathbf{p},\mathbf{p}') C_R^{\alpha,s\dagger}(\mathbf{p}) C_R^{\beta,t\dagger}(-\mathbf{p}) C_R^{\gamma,i}(-\mathbf{p}') C_R^{\delta,j}(\mathbf{p}') \\ & \times \epsilon_{\alpha\beta 3}\epsilon_{\gamma\delta 3}\epsilon_{st}\epsilon_{ij} \\ & + R \to L, \end{aligned} \tag{8}$$

with

$$\begin{aligned} D(\mathbf{p},\mathbf{p}') &= \frac{d(|\mathbf{p}-\mathbf{p}'|^2)}{|\mathbf{p}-\mathbf{p}'|^2} \\ &= \frac{Z_g\left(|\mathbf{p}-\mathbf{p}'|^2 + a\right)}{|\mathbf{p}-\mathbf{p}'|^4 + \alpha|\mathbf{p}-\mathbf{p}'|^2 + \beta}. \end{aligned} \tag{9}$$

Here $C_{R(L)}^{\dagger\alpha,s}/C_{R(L)}^{\alpha,s}$ denotes the creation/annihilation operator of a right(left)-handed particle with color α and flavor s, $e_{\mathbf{p}} \equiv \sqrt{|\mathbf{p}|^2 + m^2}$, $\alpha, \beta, \gamma, \delta$ denote color indices, i, j, s, t denote flavor indices.

The present study is performed in the chiral limit($m \to 0$). In the chiral limit, we have $e_{\mathbf{p}} = \mathbf{p}$ and $p_F = \mu$.

Because the quarks bearing the third color are free particles, we choose a variational wave function $|\Psi\rangle$ for 2SC of the form,

$$|\Psi\rangle = \Psi_L^\dagger \Psi_R^\dagger |0\rangle, \tag{10}$$

where

$$\Psi_R^\dagger = \prod_{\mathbf{p}}[u_{\mathbf{p}} + v_{\mathbf{p}} C_R^{\dagger\alpha,s}(\mathbf{p}) C_R^{\dagger\beta,t}(-\mathbf{p})\epsilon_{\alpha\beta 3}\epsilon_{st}], \tag{11}$$

$$\Psi_L^\dagger = R \to L, \tag{12}$$

Here, the color indices α and β run from 1 to 2, and the parameters obey the constraint that

$$u_{\mathbf{p}}^2 + v_{\mathbf{p}}^2 = 1. \tag{13}$$

To find the BCS state, we perform the inverse Bogoliubov -Valatin transformation. We note that a diquark condensate consists of two quarks bearing the same helicity but different color and flavor. Four kinds of quasiparticles exist, reflecting four kinds of relevant quarks. The transformation is given by

$$\begin{bmatrix} C^{11}_{R(L)}(\mathbf{p}) \\ C^{22\dagger}_{R(L)}(-\mathbf{p}) \end{bmatrix} = \begin{bmatrix} u_{\mathbf{p}} & v_{\mathbf{p}} \\ -v_{\mathbf{p}} & u_{\mathbf{p}} \end{bmatrix} \begin{bmatrix} a^1_{R(L)}(\mathbf{p}) \\ a^{2\dagger}_{R(L)}(-\mathbf{p}) \end{bmatrix}, \tag{14}$$

and

$$\begin{bmatrix} C^{12}_{R(L)}(\mathbf{p}) \\ C^{21\dagger}_{R(L)}(-\mathbf{p}) \end{bmatrix} = \begin{bmatrix} u_{\mathbf{p}} & v_{\mathbf{p}} \\ -v_{\mathbf{p}} & u_{\mathbf{p}} \end{bmatrix} \begin{bmatrix} a^3_{R(L)}(\mathbf{p}) \\ a^{4\dagger}_{R(L)}(-\mathbf{p}) \end{bmatrix}, \tag{15}$$

where $a^\dagger_{R(L)}/a_{R(L)}$ is creation/annihilation operator that creates/annihilates a quasiparticle of right-handed(left-handed) type.

The Hamiltonian $\hat{H}_S$ of the two-flavor superconductor in the quasiparticle basis is given by

$$\begin{aligned} \hat{H}_S = \sum_p \Bigg[& \begin{pmatrix} a^{1\dagger}_R(\mathbf{p}) & a^2_R(-\mathbf{p}) \end{pmatrix} \boldsymbol{D} \begin{pmatrix} a^1_R(\mathbf{p}) \\ a^{2\dagger}_R(-\mathbf{p}) \end{pmatrix} \\ & + \begin{pmatrix} a^{3\dagger}_R(\mathbf{p}) & a^4_R(-\mathbf{p}) \end{pmatrix} \boldsymbol{D} \begin{pmatrix} a^3_R(\mathbf{p}) \\ a^{4\dagger}_R(-\mathbf{p}) \end{pmatrix} \Bigg] \\ & + (R \to L) \\ & + \Delta_{\mathbf{p}} \langle C^\dagger(\mathbf{p}) C^\dagger(-\mathbf{p}) \rangle, \end{aligned} \tag{16}$$

where

$$\boldsymbol{D} \equiv \begin{bmatrix} u_{\mathbf{p}} & v_{\mathbf{p}} \\ -v_{\mathbf{p}} & u_{\mathbf{p}} \end{bmatrix} \begin{bmatrix} e_{\mathbf{p}} - \mu & -\Delta_{\mathbf{p}} \\ -\Delta_{\mathbf{p}} & -(e_{\mathbf{p}} - \mu) \end{bmatrix} \begin{bmatrix} u_{\mathbf{p}} & -v_{\mathbf{p}} \\ v_{\mathbf{p}} & u_{\mathbf{p}} \end{bmatrix}. \tag{17}$$

Here, we introduce a gap function $\Delta_{\mathbf{p}}$:

$$\Delta_{\mathbf{p}} \equiv \frac{K}{3} g^2 \sum_{\mathbf{p}'} D(\mathbf{p}, \mathbf{p}') \langle \Psi | C^{\alpha,s}_{R(L)}(-\mathbf{p}') C^{\beta,t}_{R(L)}(\mathbf{p}') \epsilon_{\alpha\beta 3}\epsilon_{st} | \Psi \rangle. \tag{18}$$

The values of the parameters $u_{\mathbf{p}}$ and $v_{\mathbf{p}}$ are chosen so that $\hat{H}_S$ has the form of free quasiparticles. After some algebra, we find that the Hamiltonian $\hat{H}_S$ is given by

$$\hat{H}_S = \Omega_g + \sum_{\mathbf{p}} \left[E_{\mathbf{p}} a^{\nu\dagger}_R(\mathbf{p}) a^\nu_R(\mathbf{p}) + (R \to L) \right], \tag{19}$$

where the superscript ν runs from 1 to 4, Ω_g is the ground state thermodynamic potential and $E_{\mathbf{p}}$ is the energy of a free quasiparticle,

$$\begin{aligned}\Omega_g &= (N_c-1)N_f\sum_{\mathbf{p}}\Big[2(e_{\mathbf{p}}-\mu)v_{\mathbf{p}}^2-2\Delta_{\mathbf{p}}u_{\mathbf{p}}v_{\mathbf{p}}\\ &\quad +\Delta_{\mathbf{p}}<C^\dagger(-\mathbf{p})C^\dagger(\mathbf{p})>\Big],\end{aligned} \tag{20}$$

and

$$E_{\mathbf{p}}\equiv\sqrt{\xi_{\mathbf{p}}^2+\Delta_{\mathbf{p}}^2}, \tag{21}$$

where $\xi_{\mathbf{p}}=e_{\mathbf{p}}-\mu=p-\mu$ and $\mu=p_F$ in the chiral limit.

In addition, we find that

$$u_{\mathbf{p}}^2 = \frac{1}{2}\left(1+\frac{\xi_{\mathbf{p}}}{E_{\mathbf{p}}}\right), \tag{22}$$

$$v_{\mathbf{p}}^2 = \frac{1}{2}\left(1-\frac{\xi_{\mathbf{p}}}{E_{\mathbf{p}}}\right), \tag{23}$$

$$u_{\mathbf{p}}v_{\mathbf{p}} = \frac{\Delta_{\mathbf{p}}}{2E_{\mathbf{p}}}. \tag{24}$$

A Cooper pair can be expressed in terms of quasiparticle operators as

$$C(-\mathbf{p})C(\mathbf{p}) = u_{\mathbf{p}}v_{\mathbf{p}}\left[1-a^\dagger(\mathbf{p})a(\mathbf{p})-a^\dagger(-\mathbf{p})a(-\mathbf{p})\right]. \tag{25}$$

Here, we ignore the particle number unconcerving processes, such as $a^\dagger a^\dagger$ and aa.

The averaged quasiparticle number is expressed by the Fermi-Dirac distribution function as

$$\begin{aligned}\langle a^\dagger(\mathbf{p})a(\mathbf{p})\rangle &= \frac{1}{1+\exp(E_{\mathbf{p}}/T)}\\ &= f_F(E_{\mathbf{p}}).\end{aligned} \tag{26}$$

The Cooper pair wave function in the mean-field $\phi(\mathbf{p})$ is given by

$$\begin{aligned}\phi(\mathbf{p}) &= \langle C(-\mathbf{p})C(\mathbf{p})\rangle\\ &= u_{\mathbf{p}}v_{\mathbf{p}}\left[1-\langle a^\dagger(\mathbf{p})a(\mathbf{p})\rangle-\langle a^\dagger(-\mathbf{p})a(-\mathbf{p})\rangle\right]\\ &= u_{\mathbf{p}}v_{\mathbf{p}}\left[1-2f_F(E_{\mathbf{p}})\right]\\ &= \frac{\Delta_{\mathbf{p}}}{2E_{\mathbf{p}}}\tanh\left(\frac{E_{\mathbf{p}}}{2T}\right).\end{aligned} \tag{27}$$

Substituting eq.(27) into eq.(18), we obtain the following gap equation at finite temperature:

$$\Delta_{\mathbf{p}}=\frac{K(N_c-1)N_f}{3}g^2\sum_{\mathbf{p}'}D(\mathbf{p},\mathbf{p}')\frac{\Delta_{\mathbf{p}'}}{2E_{\mathbf{p}'}}\tanh\left(\frac{E_{\mathbf{p}'}}{2T}\right). \tag{28}$$

In the QCD-like theory, the one-loop running coupling ($\bar{g}$) is introduced instead of the coupling constant (g) for the quark-gluon vertex with an infrared regularization parametor (p_R):

$$g^2\to\bar{g}^2(p^2)=\frac{2\pi^2 b}{\log[(p^2+p_R^2)/\Lambda_{QCD}^2]}, \tag{29}$$

where

$$b = \frac{6(N_c^2 - 1)}{2N_c(11 - 2N_f/3)}. \tag{30}$$

In the present study, $N_c = 3$ and $N_f = 2$.

It should be noted that the asymptotic freedom in the UV region is satisfied by adopting the running coupling $\bar{g}$.

Finally, we obtain the gap equation at finite temperature:

$$\Delta_{\mathbf{p}} = \frac{K(N_c - 1)N_f}{3} \sum_{\mathbf{p}'} \bar{g}^2(\mathbf{p}, \mathbf{p}') D(\mathbf{p}, \mathbf{p}') \frac{\Delta_{\mathbf{p}'}}{2E_{\mathbf{p}'}} \tanh\left(\frac{E_{\mathbf{p}'}}{2T}\right). \tag{31}$$

Ⅲ. Coherence length η

In this section, we give the expressions of coherence length η, and averaged interquark distance (d) of the relevant quarks in the present model. Cooper pair wave function at finite temperature is given by

$$\begin{aligned} \phi(\mathbf{r}) &= \int \frac{d^3p}{(2\pi)^3} \mathrm{e}^{-i\mathbf{p}\cdot\mathbf{r}} \phi(\mathbf{p}) \\ &= \int_0^\infty \frac{p^2 dp}{4\pi^2} j_0(pr) \frac{\Delta_{\mathbf{p}}}{E_{\mathbf{p}}} \tanh\left(\frac{E_{\mathbf{p}}}{2T}\right), \end{aligned} \tag{32}$$

where $j_0(pr) = \frac{\sin(pr)}{pr}$ is the zeroth-order spherical Bessel function of the 1st kind with $p = |\mathbf{p}|$ and $r = |\mathbf{r}|$.

The coherence length η, which is defined by the squared mean distance of two paired particles, can be calculated as[23],

$$\eta = \left(\frac{\int d^3r |\phi(\mathbf{r})|^2 r^2}{\int d^3r |\phi(\mathbf{r})|^2}\right)^{\frac{1}{2}}. \tag{33}$$

Ⅳ. Thermodynamic potential

In this section, we derive the thermodynamic potential Ω at finite temperature.

The Hamiltonian $\hat{H}$ including the free particles bearing the third color is given by

$$\hat{H} = \hat{H}_S + \hat{H}_3, \tag{34}$$

where $\hat{H}_3$ is the Hamiltonian of the quarks bearing the 3rd color:

$$\hat{H}_3 = \sum_{\mathbf{p}} \xi_{\mathbf{p}} C_R^{\dagger 3,s}(\mathbf{p}) C_R^{3,s}(\mathbf{p}) + R \to L, \tag{35}$$

with $C_{R(L)}^{\dagger 3,s}/C_{R(L)}^{3,s}$ denotes the creation/annihilation operator of a right(left)-handed particle with color 3 and flavor s.

The partition function Z is given by

$$\begin{aligned} Z &= \mathrm{Tr}\ \exp\left(-\frac{\hat{H}_S+\hat{H}_3}{T}\right) \\ &= \exp\left(-\frac{\Omega_g}{T}\right) \\ &\quad \times \mathrm{Tr}\ \exp\left(\frac{-\sum_{\mathbf{p}}\left[E_{\mathbf{p}}a_R^{\nu\dagger}(\mathbf{p})a_R^{\nu}(\mathbf{p})+\xi_{\mathbf{p}}C_R^{\dagger 3,s}(\mathbf{p})C_R^{3,s}(\mathbf{p})+(R\to L)\right]}{T}\right) \\ &= \exp\left[-\frac{\Omega_g}{T}\right]\cdot\left[\prod_{\mathbf{p}}\sum_{n=0}^{n=1}\exp\left(-\frac{n\cdot E_{\mathbf{p}}}{T}\right)\right]^{2(N_c-1)N_f}\cdot\left[\prod_{\mathbf{p}}\sum_{n=0}^{n=1}\exp\left(-\frac{n\cdot\xi_{\mathbf{p}}}{T}\right)\right]^{2N_f} \\ &= \exp\left[-\frac{\Omega_g}{T}\right]\cdot\prod_{\mathbf{p}}\left[1+\exp\left(-\frac{E_{\mathbf{p}}}{T}\right)\right]^{2(N_c-1)N_f}\cdot\prod_{\mathbf{p}}\left[1+\exp\left(-\frac{\xi_{\mathbf{p}}}{T}\right)\right]^{2N_f}. \end{aligned} \tag{36}$$

Then, the thermodynamic potential Ω is given by

$$\begin{aligned} \Omega &= -T\ln Z \\ &= \Omega_g - 2(N_c-1)N_fT\sum_{\mathbf{p}}\ln\left[1+\exp\left(-\frac{E_{\mathbf{p}}}{T}\right)\right] \\ &\quad -2N_fT\sum_{\mathbf{p}}\ln\left[1+\exp\left(-\frac{\xi_{\mathbf{p}}}{T}\right)\right], \end{aligned} \tag{37}$$

where

$$\begin{aligned} \Omega_g &= (N_c-1)N_f\sum_{\mathbf{p}}\left[2(e_{\mathbf{p}}-\mu)|v_{\mathbf{p}}|^2-2\Delta_{\mathbf{p}}u_{\mathbf{p}}v_{\mathbf{p}}\right] \\ &\quad +\Delta_{\mathbf{p}}<C^{\dagger}(-\mathbf{p})C^{\dagger}(\mathbf{p})> \\ &= (N_c-1)N_f\sum_{\mathbf{p}}\left[\xi_{\mathbf{p}}-E_{\mathbf{p}}+\Delta_{\mathbf{p}}\langle C^{\dagger}(-\mathbf{p})C^{\dagger}(\mathbf{p})\rangle\right] \\ &= (N_c-1)N_f\sum_{\mathbf{p}}\left[\xi_{\mathbf{p}}-E_{\mathbf{p}}+\frac{\Delta_{\mathbf{p}}^2}{2E_{\mathbf{p}}}\tanh\left(\frac{E_{\mathbf{p}}}{2T}\right)\right]. \end{aligned} \tag{38}$$

V. Quark density and Occupation number

In this section, we give expressions quark density and then, derive a relationship of the thermodynamic potential with the occupation number.

Quark density ρ is a integration of occupation number $n(\mathbf{p})$ with respect to momentum p :

$$\rho = \int\frac{d^3p}{(2\pi)^3}n(\mathbf{p}). \tag{39}$$

The same quark density ρ can be calculated from thermodynamic potential Ω as follows :

$$\rho = -\frac{\partial\Omega}{\partial\mu}. \tag{40}$$

Then, we have

$$-\frac{\partial\Omega}{\partial\mu} = \int \frac{d^3p}{(2\pi)^3} n(\mathbf{p}). \tag{41}$$

Averaged interparticle distance d of the relevant quarks is given by

$$d \sim \left(\frac{1}{\rho}\right)^{\frac{1}{3}}. \tag{42}$$

VI. Numerical calculations

In this section, after obtaining the momentum-dependent pair wave function by solving the gap equation, we calculate the coherence length η of quark Cooper pairs and several thermodynamic quantities in the chiral limit ($m = 0$). To evaluate the effect of the LQB gluon propagator, we perform the calculations in two kinds of systems. One is a system with a tree-level gluon propagator (model A), the other is a system with the LQB gluon propagator (model B). For the numerical calculation, we set the values of Λ_{QCD} and the infrared regulator(p_R) in the running coupling to 0.738 GeV and 0.776 GeV (i.e.,$\log(p_R^2/\Lambda_{QCD}^2) = 0.1$), respectively[10].

In addition, we set the value of the coefficient K to $\frac{1}{4}$. Then, as seen below, we obtain a reasonable value of the coherence length. Our result is very close to that of another study, which includes Debye mass screening effect[24]. Furthermore, the ratio $2\Delta^{T=0}_{p=p_F}/(k_B T_c)$ in our model has a very close value to the famous BCS result.

Since $(p-p')^2$ in the propagator is a gluon momentum, the most natural form of the running coupling and the propagator would be $\bar{g}^2((p-p')^2)$ and $D((p-p')^2)$, respectively. However, the momentum dependence would bring about many difficulties in actual numerical calculations. Therefore, assuming that the effect of the angle dependent part $-2pp'\cos\theta$ in $(p-p')^2$ is negligible on average, we approximate the running coupling and the propagator as[10],

$$\bar{g}^2(p,p') \approx \bar{g}^2(p^2+p'^2), \tag{43}$$
$$D(p,p') \approx D(p^2+p'^2). \tag{44}$$

Most of our numerical calculations are performed at $\mu = 0.35$ GeV. Because the region between $\mu = 0.3$ GeV and $\mu = 0.4$ GeV is the most probable area for existence of 2SC. In high-μ region, strangeness is important. As the value of μ decreases, strangeness becomes unimportant. Accordingly, in low to moderate-μ region, especially near the chiral symmetry restorating point, chirally symmetric quark matter may lie in a 2SC phase that is made up of only up and down quarks.

The diquark energy gaps Δ at $p = p_F$ in model A (Δ_A) and model B (Δ_B) at $\mu = 0.35$ GeV as functions of T are displayed in Figure 3. Δ_B has a higher amplitude than Δ_A at each T. The values of Δ_A and Δ_B decrease monotonically as T grows and vanish at $T = 0.0125$ GeV and $T = 0.0245$ GeV, respectively. The values of $2\Delta^{T=0}_{p=p_F}/(k_B T_c)$ are 3.31 in model A and 3.43 in model B, where k_B is the Boltzmann constant. $k_B = 1$ in the present study.

Figure 4 displays diquark energy gaps $\Delta_A(p)$ and $\Delta_B(p)$ at $(T,\mu) = (0, 0.35)$ GeV as functions of p apart from unimportant normalization constant. The two lines cross at $p = 0.125$ GeV and $\Delta_A(p) < \Delta_B(p)$ at higher p. These two gaps decrease monotonically as p increases and vanish at about $p = 1.0$ GeV.

Figure 5 displays Cooper pair wave functions $\Phi_A(p)$ (model A) and $\Phi_B(p)$ (model B) in momentum space at $(T,\mu) = (0, 0.35)$ GeV. The functions cross at $p = 0.125$ GeV, and

$\Phi_A(p)<\Phi_B(p)$ at larger p. These two functions exhibit a strong enhancement at $p = p_F$. The crossing point is located at the same momentum as in the $\Delta(p)$ functions (Fig.4).

Figure 6 displays Cooper pair wave functions $|\Phi_A(r)|$ and $|\Phi_B(r)|$ in co-ordinate space at $(T, \mu) = (0.01, 0.35)$ GeV, where r is a relative distance. The values of $\Phi(r)$ decreases as r increases and vanish at about $r \sim 2.0$ fm. We can see that the function $|\Phi_B(r)|$ is deviated to short distance in comparison with $|\Phi_A(r)|$.

Figure 7 shows coherence lengths η_A, η_B and averaged interquark distance d as functions of T at $\mu = 0.35$ GeV. The coherence lengths are almost constant up to T_c and $d>\eta_A>\eta_B$ below T_c.

In Figure 8, the dotted line shows occupation number $n(p)$ as a function of p at $(T, \mu) = (0, 0.35)$ GeV in model B. The quarks bearing the third color is ignored. This fact is reflected in the scale of the vertical axis (2 helicities$\times$2 flavours$\times$2 colors= 8 degrees of freedom). The true line shows the Fermi-Dirac distribution at $T = 0$. We can see that, as is well known in the ordinary BCS theory, the occupation numbers do not take the form of a Fermi-Dirac step-like function, because Cooper pairs of fermions with momenta above and below μ smear the Fermi surface and consequently transform the step-shaped line into continuous line at the Fermi momentum ($p_F = \mu$).

Figure 9 shows a quark density ρ/ρ_0 vs T at $\mu = 0.35$ GeV in model B. The value of ρ is within the realistic density as a compact star core ($\rho \sim 2.4\rho_0$, where ρ_0 denotes nuclear matter density).

Figure 10 displays the critical temperatures $T_c(A)$ and $T_c(B)$ as functions of μ. The $T_c(A)$ line forms a concave line and reaches zero at $\mu = 0.6$ GeV. While, the $T_c(B)$ line takes a form of a convex function and has a finite value at $\mu = 0.6$ GeV. In this study, realizability of the hadronic phase is ignored.

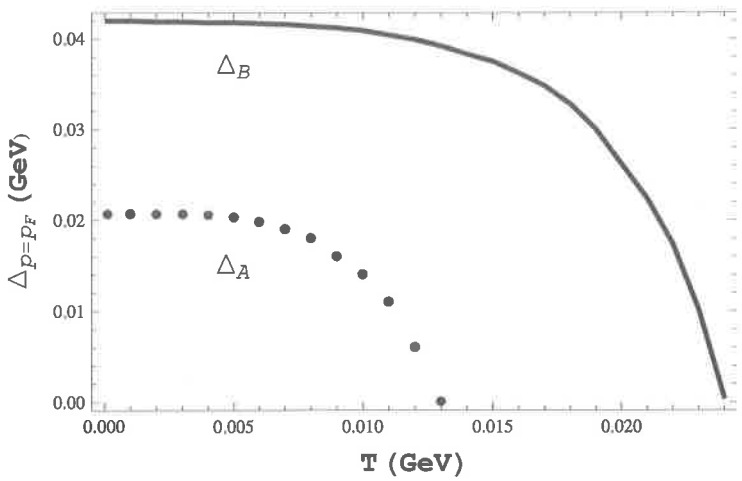

Figure 3: Diquark energy gaps Δ at $p = p_F$ in model A (Δ_A) and model B (Δ_B) with $\mu = 0.35$ GeV as functions of T. The value of Δ_A vanishes at $T = 12.5$ MeV. While, Δ_B has higher amplitude and critical temperature ($T_c = 24.5$ MeV).

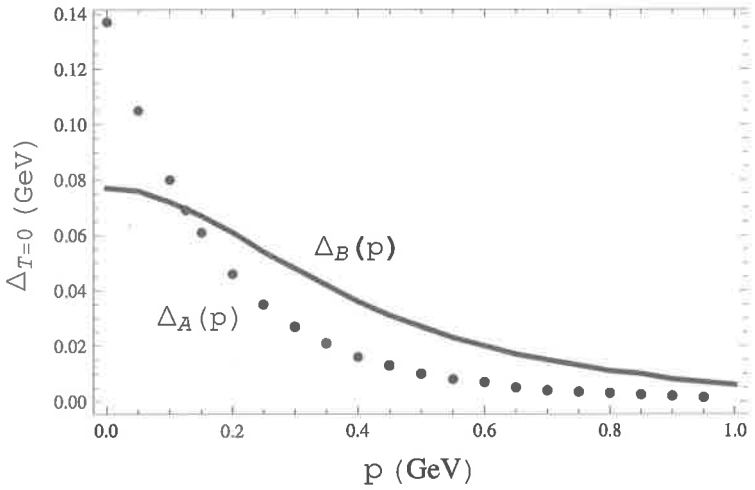

Figure 4: Diquark energy gaps Δ_A and Δ_B at $(T, \mu) = (0, 0.35)$ GeV as functions of p. The two lines cross at $p = 0.125$ GeV and $\Delta_A < \Delta_B$ at larger p.

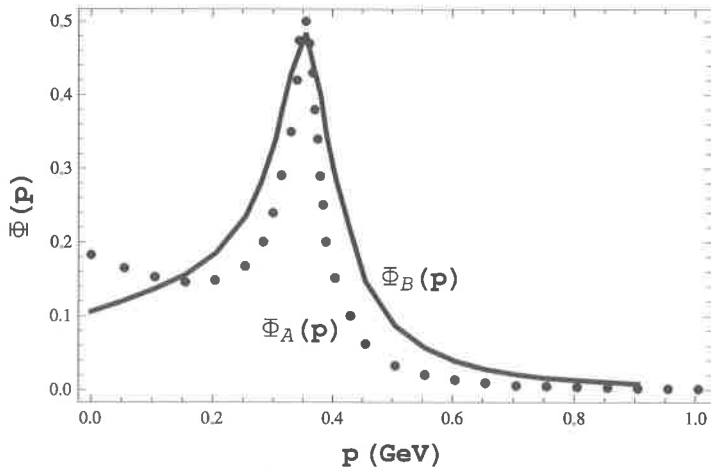

Figure 5: Cooper pair wave functions $\Phi_A(p)$ (model A) and $\Phi_B(p)$ (model B) in momentum space at $(T, \mu) = (0, 0.35)$ GeV apart from unimportant normalization constant. With these results,. The functions cross at $p = 0.125$ GeV, and $\Phi_A(p) < \Phi_B(p)$ at larger p. These two functions exhibit a strong enhancement at $p = p_F$.

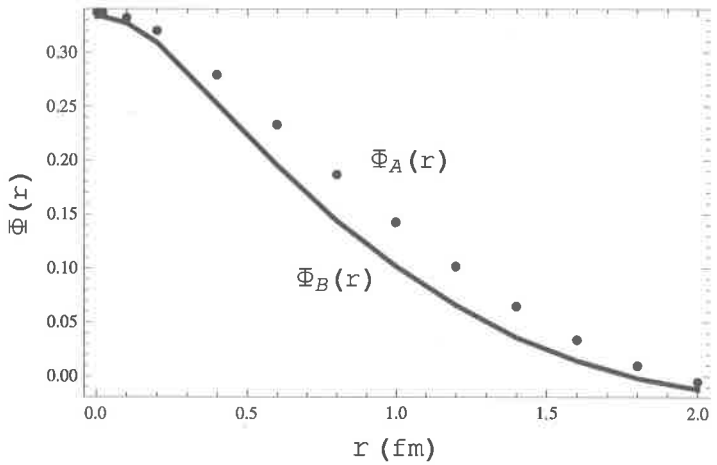

Figure 6: Cooper pair wave functions $|\Phi_A(r)|$ and $|\Phi_B(r)|$ in co-ordinate space at $(T, \mu) = (0.01, 0.35)$ GeV. $|\Phi_B(r)|$ is deviated to short distance in comparison with $|\Phi_A(r)|$. The two functions vanish at $r \sim 2$fm.

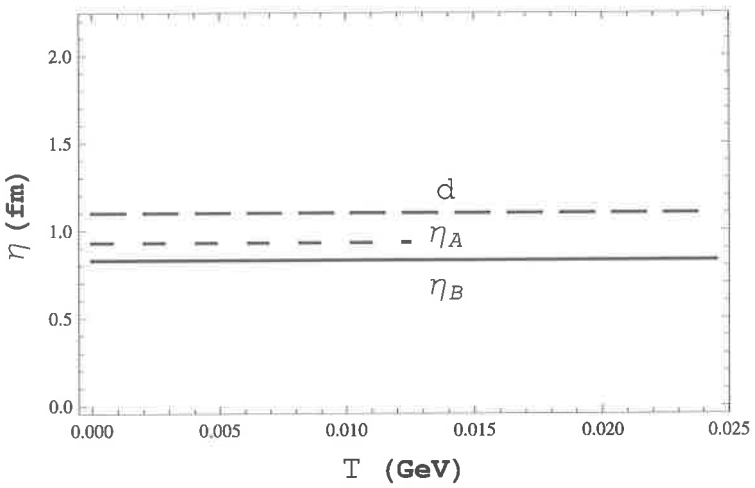

Figure 7: Coherence lengths η_A, η_B and averaged interquark distance d as functions of T at $\mu = 0.35$ GeV. The coherence lengths are almost constant up to T_c and $d > \eta_A > \eta_B$ below T_c.

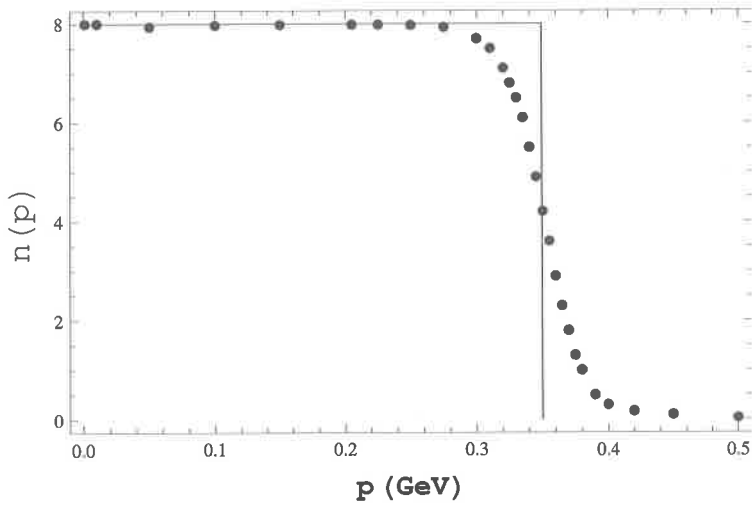

Figure 8: The doted line shows the occupation number $n(p)$ as a function of p at $(T, \mu) = (0, 0.35)$ GeV in model B without quarks bearing the third color. The true line shows the Fermi-Dirac step-like distribution.

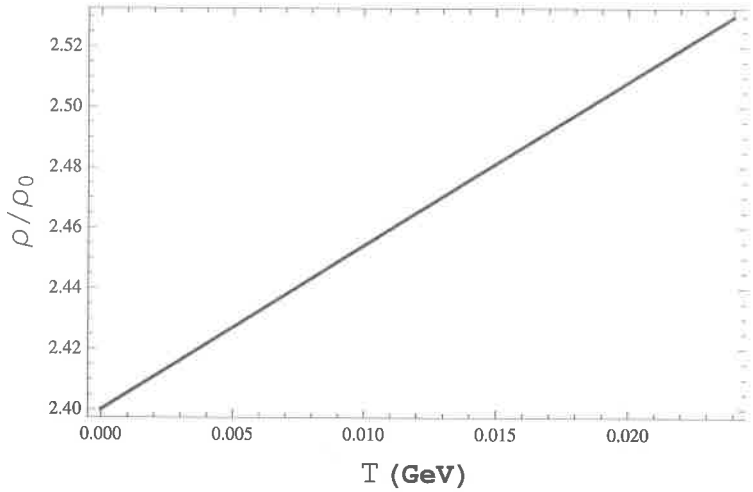

Figure 9: Quark density ρ/ρ_0 vs T at $\mu = 0.35$ GeV in model B. ρ_0 : nuclear matter density.

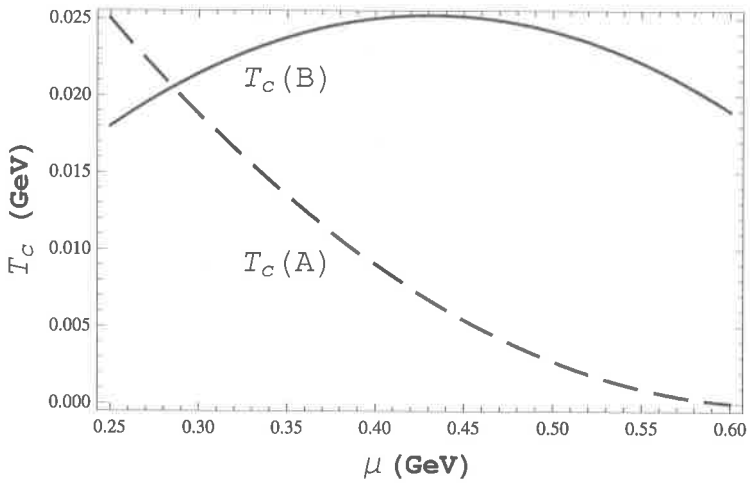

Figure 10: Critical temperatures $T_c(A)$ and $T_c(B)$ as functions of μ. The $T_c(A)$ line takes a form of a concave function and reaches zero at $\mu = 0.6$ GeV. While, the $T_c(B)$ line takes a form of a convex function and has a finite value at $\mu = 0.6$ GeV. In the figure, realizability of the hadronic phase is ignored.

Ⅶ. Conclusion

We have investigated the thermodynamics of two-flavor color superconductor at finite temperature (T) and quark chemical potential (μ) within the framework of a QCD-like effective theory with a tree-level gluon propagator (model A) and with the lattice-QCD based (LQB) gluon propagator (model B). Then, we have evaluated the effect of LQB gluon propagator on thermodynamics of two-flavor color superconductor (2SC).

Most of our numerical calculations are performed at $\mu = 0.35$ GeV. Because the region between $\mu = 0.3$ GeV and $\mu = 0.4$ GeV is the most probable area for existence of 2SC.

We have introduced an arbitrary coefficient K into our model instead of Debye screening mass and other quark density dependent factors, which weeken the quark-quark coupling strength. Expecting that the coefficient may compensate for exclusion of the effects of Debye screening and quark density on the coupling strength, we have set the value of K to $\frac{1}{4}$, then we have found that the coherence length in our model is about 1fm. Our numerical result is almost the same as the result in another study, which includes Debye mass screening effect[24]. Furthermore, we have found that the ratio $2\Delta^{T=0}_{p=p_F}/(k_B T_c)$ (Δ:energy gap, k_B:Boltzmann constant, T_c:critical temperature) in our model has a very close value to the famous BCS result. We have $2\Delta^{T=0}_{p=p_F} = 3.43 k_B T_c$ in model B. This ratio Δ/T_c is very close to the famous BCS result, which is $2\Delta = 3.52 k_B T_c$.

The entropies of the two systems (model A and B) change continuously at T_c and consequently, the latent heat is not generated. This result means that the phase transiton between 2SC and a normal quark matter, which is considered to be a quark-gluon plasma (QGP) is a second-order one.

The coherence lengths are almost constant up to T_c and $d{>}\eta_A{>}\eta_B$ below T_c. While Δ decreases as T increases and vanishes at T_c. In addition, we have found that the Cooper pair wave function $\Phi(p)$ is not affected by T, apart from normalization constant. With these results, the second-order phase transition between 2SC and QGP can be characterized by the constant spatial structure of a Cooper pair and decrease in the coherent Cooper pair number with increased T.

The small size of the Cooper pair suggests that they are tightly bound and rather bosonic. Therefore, it is natural that we expect the realizability of quark Bose-Einstein condensation phase.

The amplitudes of $\Phi(p)$ and $\Delta(p)$ in model B are larger than those in model A at $p > 0.125$ GeV, and the region of μ that 2SC possibly exist in model B is wider than that in model A.

Some of our results, the larger Δ, higher T_c, wider μ region and shorter η in model B suggest that the LQB gluon propagator induces stronger quark-quark interaction than the tree-level one.

Ⅷ. Appendix

In this appendix, we derive the Fierz-rearranged Hamiltonian with single-gluon exchange interaction for 2SC and the entropy at T_C.

Ⅷ.1 Fierz rearrangement

Our effective Hamiltonian with single-gluon exchange interaction is

$$H_I = \frac{Kg^2}{2}\int d^3x d^3y \overline{\Psi}(x)\gamma_\mu \frac{\lambda^A}{2}\Psi(x) D(x-y)\overline{\Psi}(y)\gamma^\mu \frac{\lambda^A}{2}\Psi(y), \tag{45}$$

where

$$D(x-y) = \int \frac{d^3q}{(2\pi)^3}\frac{1}{q^2}\mathrm{e}^{-iq(x-y)}. \tag{46}$$

Diquark condensate induced by single-gluon exchange is made up of identical fermions with the same helicity, antisymmetry in flavor and in color, forming a $\overline{3}$.

An effective diquark interaction is obtained by first transposing and then performing the Fierz rearrangement. Due to the tensor product structure of the matrices, one has to transform separately the color, flavor and Dirac parts by using appropriate identities to each of them.

As a first step, noting that $C\gamma^\mu C^\dagger = -(\gamma^\mu)^T$, we transpose the latter half of the above Hamiltonian, accounting for the fact that fermion fields anticommute, which generates an additional (-1) in the Hamiltonian. Then, we have

$$H_I = \frac{Kg^2}{2}\int d^3x d^3y \overline{\Psi}(x)\gamma_\mu \frac{\lambda^A}{2}\Psi(x) D(x-y)\Psi^T(y)C\gamma^\mu C^\dagger \frac{(\lambda^A)^T}{2}\overline{\Psi}^T(y), \tag{47}$$

where C is the charge-conjugation matrix $(i\gamma^2\gamma^0)$ and the superscript T stands for transposition.

As a second step, we transform the Hamiltonian with regerd to the Gell-Mann matrices, the flavor matrix and the γ matrices as follows.

Ⅷ.1.1 Gell-Mann matrices

$$\begin{aligned} I_1 &= \left[\overline{\Psi}_1^\alpha(x) T^A_{\alpha\beta}\Psi_2^\beta(x)\right]\cdot\left[\Psi_4^\delta(y)T^A_{\gamma\delta}\overline{\Psi}_3^\gamma(y)\right] \\ &= -\left[\overline{\Psi}_1^\alpha(x)\overline{\Psi}_3^\gamma(y)\right]\cdot\left[\Psi_4^\delta(y)T^A_{\gamma\delta}T^A_{\alpha\beta}\Psi_2^\beta(x)\right], \end{aligned} \tag{48}$$

where $T = \frac{\lambda}{2}$.

Using an identity,

$$\begin{aligned} T^A_{\gamma\delta}T^A_{\alpha\beta} &= \frac{1}{2}\delta_{\gamma\beta}\delta_{\alpha\delta} - \frac{1}{2N_C}\delta_{\gamma\delta}\delta_{\alpha\beta} \\ &= \frac{1}{3}\left(\delta_{\gamma\beta}\delta_{\alpha\delta} - \delta_{\gamma\delta}\delta_{\alpha\beta}\right) + \frac{1}{6}\left(\delta_{\gamma\beta}\delta_{\alpha\delta} - \delta_{\gamma\delta}\delta_{\alpha\beta}\right) \\ &= \frac{1}{3}\epsilon_{\alpha\gamma\eta}\epsilon_{\delta\beta\eta} + \frac{1}{6}\left(\delta_{\gamma\beta}\delta_{\alpha\delta} - \delta_{\gamma\delta}\delta_{\alpha\beta}\right), \end{aligned} \tag{49}$$

we select the color antisymmetric structure I_1' that is made up of two colors:

$$I_1' = -\frac{1}{3}\left[\overline{\Psi}_1^\alpha(x)\overline{\Psi}_3^\gamma(y)\epsilon_{\alpha\gamma 3}\right]\cdot\left[\Psi_4^\delta(y)\Psi_2^\beta(x)\epsilon_{\delta\beta 3}\right]. \tag{50}$$

Ⅷ.1.2 Flavor matrix

$$\begin{aligned} I_2 &= \left[\overline{\Psi}_1^s(x)\delta_{st}\Psi_2^t(x)\right]\cdot\left[\Psi_4^m(y)\delta_{lm}\overline{\Psi}_3^l(y)\right] \\ &= -\left[\overline{\Psi}_1^s(x)\overline{\Psi}_3^l(y)\right]\cdot\left[\Psi_4^m(y)\delta_{lm}\delta_{st}\Psi_2^t(x)\right]. \end{aligned} \tag{51}$$

The Kronecker delta is related to the Levi-Civita antisymmetric symbol ϵ as

$$\delta_{lm}\delta_{st} = 2\epsilon_{ls}\epsilon_{mt} + \tau^a_{lm}\tau^a_{st}, \tag{52}$$

where

$$\tau^1 = \begin{bmatrix} 0 & 1 \\ 1 & 0 \end{bmatrix},\ \tau^2 = \begin{bmatrix} 0 & -i \\ i & 0 \end{bmatrix},\ \tau^3 = \begin{bmatrix} 1 & 0 \\ 0 & -1 \end{bmatrix}. \tag{53}$$

We select the flavor antisymmetric structure I_2':

$$I_2' = -2\left[\overline{\Psi}_1^s(x)\overline{\Psi}_3^l(y)\epsilon_{ls}\right]\cdot\left[\Psi_4^m(y)\Psi_2^t(x)\epsilon_{mt}\right]. \tag{54}$$

Ⅷ.1.3 Gamma matrices

$$\begin{aligned} I_3 &= \left[\overline{\Psi}_1^i(x)\gamma_{\mu,ij}\Psi_2^j(x)\right]D(x-y)\left[\{\Psi_4(y)C\}^k\gamma^\mu_{kl}\{C^\dagger\overline{\Psi}_3(y)\}^l\right] \\ &= -D(x-y)\left[\overline{\Psi}_1^i(x)\{C^\dagger\overline{\Psi}_3(y)\}^l\right]\left[\gamma_{\mu,ij}\gamma^\mu_{kl}\{\Psi_4(y)C\}^k\Psi_2^j(x)\right] \end{aligned} \tag{55}$$

Using an identity[25],

$$\gamma_{\mu,ij}\gamma^\mu_{kl} = -(\gamma_5)_{il}(\gamma_5)_{kj} + 1 - \frac{1}{2}(\gamma^\mu\gamma_5)_{il}(\gamma_\mu\gamma_5)_{kj} - \frac{1}{2}(\gamma^\mu)_{il}(\gamma_\mu)_{kj}, \tag{56}$$

we select the Lorentz scalar structure I_3':

$$I_3' = D(x-y)\left[\overline{\Psi}_1^i(x)(\gamma_5)_{il}\{C^\dagger\overline{\Psi}_3(y)\}^l\right]\left[\{\Psi_4(y)C\}^k(\gamma_5)_{kj}\Psi_2^j(x)\right]. \tag{57}$$

As a third step, we collect the Lorentz scalar, color antisymmetric and flavor antisymmetric terms and multiply them.

$$I' = \frac{1}{3}\times 2\times(-1)\left[-D(x-y)\overline{\Psi}_s^\alpha(x)C^\dagger\gamma_5\overline{\Psi}_t^{T\beta}(y)\epsilon_{\alpha\beta3}\epsilon^{st}\right]\left[\Psi_l^{T\gamma}(y)C\gamma_5\Psi_m^\delta(x)\epsilon_{\gamma\delta3}\epsilon^{lm}\right], \tag{58}$$

where $\gamma^5 = i\gamma^0\gamma^1\gamma^2\gamma^3$ and $\gamma_5 C^\dagger = C^\dagger\gamma_5$.

Ⅷ.1.4 Fourier transformation

Using Fourier transformation, we can derive the Hamiltonian in three-momentum space as below,

$$\overline{\Psi}_s^\alpha(x) = \int\frac{d^3p'}{(2\pi)^3}\overline{\Psi}_s^\alpha(p')e^{ip'x}. \tag{59}$$

$$\overline{\Psi}_t^{T\beta}(y) = \int\frac{d^3k'}{(2\pi)^3}\overline{\Psi}_t^{T\beta}(k')e^{ik'y}. \tag{60}$$

$$\Psi_l^{T\gamma}(y) = \int \frac{d^3k}{(2\pi)^3} \Psi_l^{T\gamma}(k) \mathrm{e}^{-iky}. \tag{61}$$

$$\Psi_m^{\delta}(x) = \int \frac{d^3p}{(2\pi)^3} \Psi_m^{\delta}(p) \mathrm{e}^{-ipx}. \tag{62}$$

Integration with respect to x and y in the co-ordinate space is immediate.

$$\begin{aligned} & \int d^3x \int d^3y \mathrm{e}^{-iq(x-y)} \cdot \mathrm{e}^{ip'x} \cdot \mathrm{e}^{ik'y} \cdot \mathrm{e}^{-iky} \cdot \mathrm{e}^{-ipx} \\ = & \int d^3x \int d^3y \mathrm{e}^{-ix(q+p-p')} \cdot \mathrm{e}^{iy(-q+k-k')} \\ = & (2\pi)^3 \delta(\mathbf{q}+\mathbf{p}-\mathbf{p}')(2\pi)^3 \delta(-\mathbf{q}+\mathbf{k}-\mathbf{k}') \end{aligned} \tag{63}$$

The resultant Hamiltonian in the momentum space is

$$\begin{aligned} \hat{H}_I = & \frac{K}{3} g^2 \int \frac{d^3q}{(2\pi)^3} \int \frac{d^3p'}{(2\pi)^3} \int \frac{d^3k'}{(2\pi)^3} \int \frac{d^3k}{(2\pi)^3} \int \frac{d^3p}{(2\pi)^3} (2\pi)^3 (2\pi)^3 \\ & \times \delta(\mathbf{q}+\mathbf{p}-\mathbf{p}') \delta(-\mathbf{q}+\mathbf{k}-\mathbf{k}') \frac{1}{q^2} \overline{\Psi}_s^{\alpha}(p') C^{\dagger} \gamma_5 \overline{\Psi}_t^{T\beta}(k') C \gamma_5 \Psi_l^{T\gamma}(k) \Psi_m^{\delta}(p) \\ & \times \epsilon_{\alpha\beta 3} \epsilon_{\gamma\delta 3} \epsilon^{st} \epsilon^{lm}. \end{aligned} \tag{64}$$

After integrating out with respect to q and k', we have

$$\begin{aligned} \hat{H}_I = & \frac{K}{3} g^2 \int \frac{d^3p'}{(2\pi)^3} \int \frac{d^3k}{(2\pi)^3} \int \frac{d^3p}{(2\pi)^3} \\ & \times \frac{1}{(p-p')^2} \overline{\Psi}_s^{\alpha}(p') C^{\dagger} \gamma_5 \overline{\Psi}_t^{T\beta}(p-p'+k) \Psi_l^{T\gamma}(k) C \gamma_5 \Psi_m^{\delta}(p) \\ & \times \epsilon_{\alpha\beta 3} \epsilon_{\gamma\delta 3} \epsilon^{st} \epsilon^{lm} \end{aligned} \tag{65}$$

Furthermore we select a zero-momentum Cooper pair, which has the lowest energy. Then, noting that a quark Cooper pair induced by single-gluon exchange is made up of quarks with the same helicity, we finally obtain the interaction Hamiltonian in momentum space:

$$\begin{aligned} \hat{H}_I = & \frac{K}{3} g^2 \int \frac{d^3p'}{(2\pi)^3} \int \frac{d^3k}{(2\pi)^3} \int \frac{d^3p}{(2\pi)^3} \\ & \times (2\pi)^3 \delta(\mathbf{p}+\mathbf{k}) \frac{1}{(p-p')^2} \overline{\Psi}_R^{\alpha,s}(p') C^{\dagger} \gamma_5 \overline{\Psi}_R^{\beta,t}(p-p'+k) \Psi_R^{\gamma,l}(k) C \gamma_5 \Psi_R^{\delta,m}(p) \\ & \times \epsilon_{\alpha\beta 3} \epsilon_{\gamma\delta 3} \epsilon_{st} \epsilon_{lm} \\ & + R \to L \\ = & \frac{K}{3} g^2 \int \frac{d^3p'}{(2\pi)^3} \int \frac{d^3p}{(2\pi)^3} \frac{1}{(p-p')^2} \overline{\Psi}_R^{\alpha,s}(p') C^{\dagger} \gamma_5 \overline{\Psi}_R^{\beta,t}(-p') \Psi_R^{\gamma,l}(-p) C \gamma_5 \Psi_R^{\delta,m}(p) \\ & \times \epsilon_{\alpha\beta 3} \epsilon_{\gamma\delta 3} \epsilon_{st} \epsilon_{lm} \\ & + R \to L. \end{aligned} \tag{66}$$

In the text, in order to simplify algebra, we neglect two factors ($C\gamma_5$ and $C^{\dagger}\gamma_5$) in the above Hamiltonian.

Ⅷ.2 Second order phase transition

In the study, we ignore interactions between quasiparticles.

Then, the entropy density S of 2SC in the present system is given by that of a free fermion system as

$$S = -2(N_c - 1)N_f \sum_{\mathbf{p}} [(1 - f_F(E_\mathbf{p}))\ln(1 - f_F(E_\mathbf{p})) + f_F(E_\mathbf{p})\ln(f_F(E_\mathbf{p}))] \,. \tag{67}$$

At the critical temperature, the entropy density changes continuously into that of a normal quark matter (quark-gluon plasma) :

$$\begin{aligned} S &= -2(N_c - 1)N_f \sum_{\mathbf{p}} [(1 - f_F(|\xi_\mathbf{p}|))\ln(1 - f_F(|\xi_\mathbf{p}|)) + f_F(|\xi_\mathbf{p}|)\ln(f_F(|\xi_\mathbf{p}|))] \\ &= -2(N_c - 1)N_f \sum_{\mathbf{p}} [(1 - f_F(\xi_\mathbf{p}))\ln(1 - f_F(\xi_\mathbf{p})) + f_F(\xi_\mathbf{p})\ln(f_F(\xi_\mathbf{p}))] \,. \end{aligned} \tag{68}$$

This means that the phase transition is the second order one.

References

1) Asakawa M, Yazaki K (1989) Chiral restoration at finite density and temperature. Nucl Phys. A504, 668-684.

2) Berges J, Rajagopal K (1999) Color Superconductivity and Chiral Symmetry Restoration at Nonzero Baryon Density and Temperature. Nucl Phys. B538, 215-232.

3) Huang M, Zhaung P, Chao W (2002) Massive quark propagator and competition between chiral and diquark condensate. Phys Rev D. 65, 076012-076045.

4) Carter GW, Diakonov D (1999) Light quarks in the instanton vacuum at finite baryon density. Phys Rev D. 60, 016004-016014.

5) Kiuchi H, Oka M (2005) Thermodynamics of two-flavor quark matter in the instanton vacuum at finite temperature. Prog Theor Phys. 114, 813-843.

6) Kiuchi H, Oka M (2006) Charge neutral two-flavor quark matter in the instanton vacuum and compact stars. Prog Theor Phys. 115, 909-929.

7) Andersen JO, Khan R, Kyllingstad LT (2011) The chiral phase transition and the role of vacuum fluctuations. hep-ph 1102.2779.

8) Taniguchi Y, Yoshida Y (1997) Chiral symmetry restoration at finite temperature and chemical potential in the improved ladder approximation. Phys Rev D. 55, 2283-2289.

9) Kiriyama O, Maruyama M, Takagi F (2000) Chiral phase transition at high temperature and density in the QCD-like theory. Phys Rev D. 62, 105008-105017.

10) Kiuchi H, Iwasaki M (2004) Latent heat in the chiral phase transition. Prog Theor Phys Suppl. 153, 313-316.

11) Tsue Y, Fujii H, Hashimoto Y (2007) Landau Potential Study of the Chiral Phase Transition in a QCD-Like Theory. Int J Mod Phys E. 16, 2276-2281.

12) Alford M (2004) Dense Quark Matter in Nature. Prog Theor Phys Suppl. 153, 1-14.

13) Alford M, Rajagopal K, Wilczek F (1999) Color-flavor locking and chiral symmetry breaking in high density QCD. Nucl Phys B. 537, 443-458.

14) Alford M (2001) Color superconducting quark matter. Ann Rev Nucl Part Sci. 51, 131-160.

15) Kogut JB, Stephanov MA (2004) The Phases of Quantum Chromodynamics,Cambridge University Press, Cambridge. 224-283.

16) Schäfer T (1998) Instantons in QCD. Rev Mod Phys. 70, 323-426.

17) Iida H, Suganuma H, Oka M (2005) Dynamical chiral-symmetry breaking at $T = 0$ and $T \neq 0$ in the Schwinger-Dyson equation with lattice QCD data. Eur Phys J A. 23, 305-315.

18) Itoh N (1970) Hydrostatic equilibrium of hypothetical quark stars. Prog Theor Phys. 44, 291-292.

19) Glendenning NK (2000) Compact Stars; Nuclear Physics, Particle Physics and General Relativity, Springer, London. 199-413.

20) Blaschke D, Voskresensky DN, Grigorian H (2001) Cooling of Hybrid Neutron Stars and Hypothetical Self-bound Objects with Superconducting Quark Cores. Astron Astrophys. 368, 561-568.

21) Alford M, Rajagopal K, Wilczek F (1998) QCD at finite baryon density;nucleon droplets and color superconductivity. Phys Lett B. 422, 247-256.

22) Bowman PO, Heller UM, Leinweber DB et al (2004) Unquenched Gluon Propagator in Landau Gauge. Phys Rev D. 70, 034509-034513.

23) De Blasio (1997) Coherence length of neutron superfluids. Phys Rev C. 56, 2332-2335.

24) Matsuzaki M (2000) Spatial structure of quark Cooper pairs in a color superconductor. Phys Rev D. 62, 017501-017504.

25) Ta-Pei Chen, Ling-Fong Li (1983) Gauge theory of elementary particle physics, Oxford university press, Oxford. 495.

（平成24年11月30日稿）

査読終了年月日　平成24年 1 月16日